

# Enhanced photodegradation activity of methyl orange over Z-scheme type MoO<sub>3</sub>-g-C<sub>3</sub>N<sub>4</sub> composite under visible light irradiation†

Cite this: *RSC Adv.*, 2014, 4, 13610

Yiming He,<sup>\*ae</sup> Lihong Zhang,<sup>a</sup> Xiaoxing Wang,<sup>a</sup> Ying Wu,<sup>b</sup> Hongjun Lin,<sup>c</sup> Leihong Zhao,<sup>b</sup> Weizheng Weng,<sup>d</sup> Huilin Wan<sup>d</sup> and Maohong Fan<sup>\*ef</sup>

Novel Z-scheme type MoO<sub>3</sub>-g-C<sub>3</sub>N<sub>4</sub> composites photocatalysts were prepared with a simple mixing-calcination method, and evaluated for their photodegradation activities of methyl orange (MO). The optimized MoO<sub>3</sub>-g-C<sub>3</sub>N<sub>4</sub> photocatalyst shows a good activity with a kinetic constant of 0.0177 min<sup>-1</sup>, 10.4 times higher than that of g-C<sub>3</sub>N<sub>4</sub>. Controlling various factors (MoO<sub>3</sub>-g-C<sub>3</sub>N<sub>4</sub> amount, initial MO concentration, and pH value of MO solution) can lead to the enhancement of the photocatalytic activity of the composite. Only MoO<sub>3</sub> and g-C<sub>3</sub>N<sub>4</sub> are detected with X-ray diffraction (XRD) and Fourier transform infrared spectroscopy (FT-IR) spectra. N<sub>2</sub> adsorption and UV-vis diffuse reflectance spectroscopy (DRS) results suggest that the addition of MoO<sub>3</sub> slightly affects the specific surface area and the photoabsorption performance. The transmission electron microscopy (TEM) image of MoO<sub>3</sub>-g-C<sub>3</sub>N<sub>4</sub> indicates a close contact between MoO<sub>3</sub> and g-C<sub>3</sub>N<sub>4</sub>, which is beneficial to interparticle electron transfer. The high photocatalytic activity of MoO<sub>3</sub>-g-C<sub>3</sub>N<sub>4</sub> is mainly attributed to the synergetic effect of MoO<sub>3</sub> and g-C<sub>3</sub>N<sub>4</sub> in electron-hole pair separation via the charge migration between the two semiconductors. The charge transfer follows direct Z-scheme mechanism, which is proven by the reactive species trapping experiment and the ·OH-trapping photoluminescence spectra.

Received 23rd January 2014  
Accepted 4th March 2014

DOI: 10.1039/c4ra00693c

www.rsc.org/advances

## 1. Introduction

Organic pollutants are present in the water environment usually as a result of industrial effluents. With the development of industry, the volume of wastewater containing nonbiodegradable pollutants have increased rapidly. Dealing with the pollutants demands the development of new, effective, clean,

and safe decontamination technologies. Photocatalysis represents a promising alternative technology for degradation of organic pollutants in water, and hence attracts much attention.<sup>1</sup> Titanium oxide (TiO<sub>2</sub>) has been used to degrade many organic pollutants in water and air.<sup>2-6</sup> It is considered as a promising photocatalyst since it is stable, insoluble, non-toxic, resistant to corrosion and relatively inexpensive. However, TiO<sub>2</sub> photocatalyst is effective only under irradiation of UV light due to its wide band gap. Many strategies, such as metal or nonmetal element doping,<sup>7-9</sup> dye sensitization<sup>10</sup> and semiconductor coupling,<sup>11</sup> have been applied to overcome the shortcoming. Cost-effective photocatalysts with high efficiencies under visible light are desired.

Currently, many scientists pay attention on the non-TiO<sub>2</sub> based photocatalyst and developed a lot of novel photocatalysts, such as Bi<sub>2</sub>WO<sub>6</sub>,<sup>12</sup> g-C<sub>3</sub>N<sub>4</sub>,<sup>13</sup> Ag<sub>3</sub>PO<sub>4</sub>,<sup>14</sup> AgBr,<sup>15</sup> etc. Among them, g-C<sub>3</sub>N<sub>4</sub> attracted a great deal of interests due to its good photoactivity, moderate band gap, and low cost. In addition, it is considered as a “sustainable” material since pure g-C<sub>3</sub>N<sub>4</sub> is a metal-free semiconductor and can be synthesized by the simple calcination of urea and melamine at 500–600 °C.<sup>16,17</sup> Three approaches have been applied to promote its photocatalytic activity in degrading organics more efficiently: increasing the surface area,<sup>18,19</sup> doping with metal or nonmetal elements,<sup>20,21</sup> coupling with another semiconductor.<sup>22,23</sup> The last method was considered as the most feasible one, which has been applied to

<sup>a</sup>Department of Materials Physics, Zhejiang Normal University, Jinhua, China. E-mail: hym@zjnu.cn; Fax: +86-0579-83714946; Tel: +86-0579-83792294

<sup>b</sup>Institute of Physical Chemistry, Zhejiang Key Laboratory for Reactive Chemistry on Solid Surfaces, Zhejiang Normal University, Jinhua, China

<sup>c</sup>College of Geography and Environmental Sciences, Zhejiang Normal University, Jinhua, China

<sup>d</sup>State Key Laboratory Physical Chemistry of Solid Surfaces, Xiamen University, Xiamen, China

<sup>e</sup>Department of Chemical & Petroleum Engineering, University of Wyoming, Laramie, Wyoming 82071, USA. E-mail: mfan@uwyo.edu; Fax: +1-307-766-6667; Tel: +1-307-766-5633

<sup>f</sup>School of Civil and Environmental Engineering, Georgia Institute of Technology, Georgia, 30332, USA. E-mail: mfan3@mail.gatech.edu; Fax: +1-404-894-8266; Tel: +1-404-385-4577

† Electronic supplementary information (ESI) available: TG-DTA profiles of pure g-C<sub>3</sub>N<sub>4</sub> and 1.5 wt% MoO<sub>3</sub>-g-C<sub>3</sub>N<sub>4</sub> composite (Fig. S1), SEM pictures of pure g-C<sub>3</sub>N<sub>4</sub>, MoO<sub>3</sub>, and 1.5 wt% MoO<sub>3</sub>-g-C<sub>3</sub>N<sub>4</sub> composite (Fig. S2). XRD patterns of 1.5 wt% MoO<sub>3</sub>-g-C<sub>3</sub>N<sub>4</sub> before and after reaction (Fig. S3). The elemental concentration in 1.5 wt% MoO<sub>3</sub>-g-C<sub>3</sub>N<sub>4</sub> photocatalyst (Table S1). See DOI: 10.1039/c4ra00693c

develop Pt/CdS/PdS composite with the highest quantum efficiency achieved so far.<sup>24</sup> Since Wang *et al.* first reported the photocatalytic activity of  $g\text{-C}_3\text{N}_4$ ,<sup>13</sup> a variety of  $g\text{-C}_3\text{N}_4$  based composite photocatalysts have been reported. A number of semiconductors, such as  $\text{WO}_3$ ,<sup>25</sup>  $\text{ZnO}$ ,<sup>26</sup>  $\text{SmVO}_4$ ,<sup>27</sup>  $\text{Bi}_2\text{WO}_6$ ,<sup>28</sup>  $\text{AgBr}$ <sup>29</sup> *etc.*, have been used as a doper to strengthen the photocatalytic activity of  $g\text{-C}_3\text{N}_4$ . The promotion effect was usually explained by three different mechanisms. The first one is sensitization in which electrons generated by visible-light irradiation in  $g\text{-C}_3\text{N}_4$  migrate to a wider bandgap semiconductor (such as  $\text{ZnO}$ ,  $\text{TiO}_2$ ,  $\text{YVO}_4$ ),<sup>26,30,31</sup> while the photogenerated holes stay in the  $g\text{-C}_3\text{N}_4$ . This would facilitate electron-hole separation, suppress charge recombination, and hence improve the photocatalytic activity. The second one is often associated with heterojunction composite photocatalyst in which both semiconductors can be excited to generate electron-hole pairs.<sup>27,28</sup> The photogenerated electrons from  $g\text{-C}_3\text{N}_4$  with a higher conduction band could transport to another semiconductor with a lower conduction band. Meanwhile, the photogenerated holes from the semiconductor with a lower valence band transport to the  $g\text{-C}_3\text{N}_4$  with a higher valence band. The double charge transfer may also lead to the separation of electrons and holes and enhance the photo-catalytic efficiency. The third one could be called as direct Z-scheme type mechanism. Taking  $g\text{-C}_3\text{N}_4/\text{TiO}_{2-x}\text{S}_x$  photocatalyst as an example, the photogenerated electrons from the  $\text{TiO}_{2-x}\text{S}_x$  semiconductor with a lower conduction band recombine with photogenerated holes from the  $g\text{-C}_3\text{N}_4$  with a higher valence band.<sup>32</sup> By this way, the electrons on  $g\text{-C}_3\text{N}_4$  and holes on  $\text{S-TiO}_2$  are separated efficiently. The  $g\text{-C}_3\text{N}_4/\text{TiO}_{2-x}\text{S}_x$  composite showed four times higher quantum efficiency than S doped  $\text{TiO}_2$  in the photodegradation of acetaldehyde.<sup>32</sup> Although all the three mechanisms have been widely used by scientists to explain their works, there are still some questions about how to choose the mechanism suitable to a specific research. The band edge potential of semiconductor is generally considered as the criterion which works well in the differentiation of the first two mechanisms. However, it is not enough to distinguish the double-charge-transfer mechanism and direct Z-scheme mechanism. More detailed works need to be done for resolving the issue.

A new Z-scheme type photocatalyst,  $\text{MoO}_3\text{-}g\text{-C}_3\text{N}_4$  composite in spite of its similarity to  $g\text{-C}_3\text{N}_4$  doped  $\text{MoO}_3$  composite,<sup>33</sup> was developed in this paper. Li *et al.*<sup>33</sup> think that the  $g\text{-C}_3\text{N}_4\text{-MoO}_3$  composite follows the double-charge-transfer mechanism. However, this research proved that the real mechanism is Z-scheme type mechanism based on the active species trapping experiment. In addition, in comparison to Li's catalyst with 93.0 wt%  $\text{MoO}_3$ , a very low content of  $\text{MoO}_3$  (1.5 wt%) was used in this work, while the latter exhibits excellent photocatalytic activity in dyes photodegradation under visible light irradiation. The high activity and low cost indicates that the  $\text{MoO}_3\text{-}g\text{-C}_3\text{N}_4$  is promising photocatalyst.

## 2. Experimental section

### 2.1 Catalysts preparation

$(\text{NH}_4)_6\text{Mo}_7\text{O}_{24}\cdot 4\text{H}_2\text{O}$  (>99.0%), melamine (99.0%), urea (99.0%), tetrabutyl titanate (>99.0%), benzoquinone (>98.0%), KI (>99.0%), isopropanol (>99.7%), coumarin (>99.0%), and

ethanol (>99.5%) were purchased and used without further purification. N-doped  $\text{TiO}_2$  was prepared by a modified sol-gel method.<sup>34</sup> Pure  $\text{MoO}_3$  was prepared by directly calcining at 500 °C for 4 h. Pure  $g\text{-C}_3\text{N}_4$  powders were prepared by directly calcining melamine in a muffle furnace. In a typical synthesis run, 6 g of melamine was placed in an alumina crucible with a cover. The crucible was heated to 520 °C for 4 h at a heating rate of 10 °C  $\text{min}^{-1}$ . After cooling to room temperature, yellow  $g\text{-C}_3\text{N}_4$  was obtained in a powder form.

The  $\text{MoO}_3\text{-}g\text{-C}_3\text{N}_4$  composites were prepared according to the following procedure. 0.03 g of  $\text{MoO}_3$  and 1.97 g of  $g\text{-C}_3\text{N}_4$  were mixed and ground in an agate mortar for 20 min. Then, the mixture was calcined at 400 °C for 2 h to obtain the 1.5 wt%  $\text{MoO}_3\text{-}g\text{-C}_3\text{N}_4$  catalyst. Other  $\text{MoO}_3\text{-}g\text{-C}_3\text{N}_4$  catalysts were prepared by a same method except the  $g\text{-C}_3\text{N}_4$  concentration.

### 2.2 Photocatalytic reaction

The photocatalytic activities of the synthesized powders were evaluated by degrading methyl orange (MO) under visible-light irradiation. The light source for photocatalysis was a spherical Xe lamp (350 W). Two optical filters were used to eliminate the UV light and infrared light (800 nm >  $\lambda$  > 420 nm). The power density at the position of reactor is about 16  $\text{mW cm}^{-2}$ . The volume of initial MO solution is 100 mL. All the powder contents in the MO aqueous solution are 0.10 g 100  $\text{mL}^{-1}$ . Prior to irradiation, the mixture was agitated for an hour to ensure adsorption-desorption equilibrium at room temperature. At regular intervals, samples were withdrawn and centrifuged to remove photocatalyst for analysis. The concentration of aqueous MO was determined by measuring its absorbance at the range of 400 nm to 700 nm. The MO degradation was calculated by Lambert-Beer equation. Photoactivity for MO under visible-light irradiation in the absence of the photocatalyst was also evaluated. The photodegradation of other dyes, rhodamine B (RhB) and methylene blue (MB), was also carried out by the similar procedure.

The examination experiment process of reactive species was similar to the photodegradation experiment. A quantity of scavengers was introduced into the MO solution prior to addition of the catalyst. The concentration of scavengers was controlled to be 0.01  $\text{mol L}^{-1}$  according to the previous studies<sup>35,36</sup> with the exception of benzoquinone (0.0001  $\text{mol L}^{-1}$ ).

The formation rate of  $\cdot\text{OH}$  at photo-illuminated sample/water interface was detected by the photoluminescence (PL) technique using coumarin (COU) as a probe molecule. The measurement was carried out in the photocatalytic testing system. In a typical run, 0.2 g of the samples was added to an aqueous solution (100 mL) containing 10 mM COU in a 250 mL beaker. After irradiation for a given time, 8 mL aliquots were sampled and centrifuged for analysis. The  $\cdot\text{OH}$  formed in the system can react with COU and generate 7-hydroxycoumarin (7HC), the fluorescence intensity of which is directly proportional to the generated  $\cdot\text{OH}$ .<sup>37</sup>

### 2.3 Characterization

Thermogravimetry analysis (TG-DTA; Netzsch STA449) was carried out in a flow of air (10  $\text{mL min}^{-1}$ ) at a heating rate of

10 °C min<sup>-1</sup>. The specific surface areas were measured on Autosorb-1 (Quantachrome Instruments) with Brunauer–Emmett–Teller (BET) method. The XRD characterization of catalysts was carried out on Philips PW3040/60 X-ray diffractometer, using Cu K $\alpha$  radiation (40 kV/40 mA). The FT-IR spectra of the catalysts were recorded on Nicolet NEXUS670 with a resolution of 4 cm<sup>-1</sup>. The X-ray photoelectron spectroscopy (XPS) measurements were performed with a Quantum 2000 Scanning ESCA Microprobe instrument using Al K $\alpha$ . The C 1s signal was set to a position of 284.6 eV. The scanning electron microscopy (SEM) pictures were taken on a field emission scanning electron microscope (LEO-1530). The TEM images were collected with a JEM-2010F transmission electron microscope at an accelerating voltage of 200 kV. The DRS spectra of catalysts were recorded on a UV-vis spectrometer (PerkinElmer Lambda900) equipped with an integrating sphere. The PL spectra were collected on FLS-920 spectrometer (Edinburgh Instrument), using a Xe lamp (excitation at 365 nm and 332 nm for photocatalyst and 7HC, respectively) as light source.

Photocurrent was measured on an electrochemical analyzer (CHI660B) in a two-electrode system under zero bias. The prepared sample and a Pt wire are used as the working electrode and the counter electrode, respectively. A 350 W Xe arc lamp through a UV-cutoff filter ( $\lambda > 420$  nm) served as a light source. Na<sub>2</sub>SO<sub>4</sub> (0.5 mol L<sup>-1</sup>) aqueous solution was used as the electrolyte. Working electrodes were prepared based on the literature reported.<sup>27</sup>

### 3. Results and discussion

#### 3.1 Characterizations of g-C<sub>3</sub>N<sub>4</sub>, MoO<sub>3</sub> and MoO<sub>3</sub>-g-C<sub>3</sub>N<sub>4</sub> composites

Thermo-gravimetric analysis was performed from room temperature to 800 °C under air conditions to determine the real content of MoO<sub>3</sub> in MoO<sub>3</sub>-g-C<sub>3</sub>N<sub>4</sub> composite. The results are shown in Fig. 1. For clarity, only the TG profiles of pure g-C<sub>3</sub>N<sub>4</sub> and three MoO<sub>3</sub>-g-C<sub>3</sub>N<sub>4</sub> composites are presented. It can be observed that the weight of pure g-C<sub>3</sub>N<sub>4</sub> decreased rapidly in the temperature range of 600–750 °C, indicating that the decomposition of g-C<sub>3</sub>N<sub>4</sub> occurred in this temperature range.

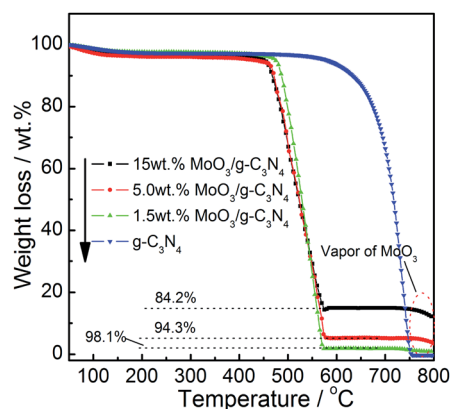


Fig. 1 TG profiles of MoO<sub>3</sub>-g-C<sub>3</sub>N<sub>4</sub> composites.

Table 1 Specific surface area and the real MoO<sub>3</sub> concentrations of MoO<sub>3</sub>-g-C<sub>3</sub>N<sub>4</sub> composites

Catalysts	S m <sup>-2</sup> g <sup>-1</sup>	MoO <sub>3</sub> content per wt%
g-C <sub>3</sub> N <sub>4</sub>	13	0
MoO <sub>3</sub>	1.7	100
1.0 wt% MoO <sub>3</sub> -g-C <sub>3</sub> N <sub>4</sub>	14.7	1.2
1.5 wt% MoO <sub>3</sub> -g-C <sub>3</sub> N <sub>4</sub>	14.4	1.9
2.0 wt% MoO <sub>3</sub> -g-C <sub>3</sub> N <sub>4</sub>	11.6	2.4
5.0 wt% MoO <sub>3</sub> -g-C <sub>3</sub> N <sub>4</sub>	7.1	5.7
15 wt% MoO <sub>3</sub> -g-C <sub>3</sub> N <sub>4</sub>	6.9	15.8

For MoO<sub>3</sub>-g-C<sub>3</sub>N<sub>4</sub> composite, the weight-loss range shift forwards to 480–570 °C, which suggests that the existence of MoO<sub>3</sub> promotes the combustion of g-C<sub>3</sub>N<sub>4</sub>, as observed in the SmVO<sub>4</sub>/g-C<sub>3</sub>N<sub>4</sub> photocatalyst.<sup>27</sup> The real concentration of MoO<sub>3</sub> can be easily calculated from the residuals after the samples were heated over 600 °C. As shown in Table 1, the real MoO<sub>3</sub> content is slightly larger than the theoretical values. Actually, the difference between the real and theoretical value of g-C<sub>3</sub>N<sub>4</sub> is usually large in the reported g-C<sub>3</sub>N<sub>4</sub> based photocatalysts.<sup>27,38,39</sup> The small difference in the MoO<sub>3</sub>-g-C<sub>3</sub>N<sub>4</sub> might be ascribed to the low preparation temperature (400 °C). Besides the weight loss of g-C<sub>3</sub>N<sub>4</sub>, another weight loss between 750 and 800 °C in the MoO<sub>3</sub>-g-C<sub>3</sub>N<sub>4</sub> composites, could be ascribed to the vaporization of MoO<sub>3</sub>. This result is consistent with the phase composition. The BET surface areas of MoO<sub>3</sub>-g-C<sub>3</sub>N<sub>4</sub> composites are also shown in Table 1. Pure MoO<sub>3</sub> exhibits much lower surface area than pure g-C<sub>3</sub>N<sub>4</sub>. However, the addition of a small amount of MoO<sub>3</sub> to g-C<sub>3</sub>N<sub>4</sub> led to the increase in the BET value of photocatalyst, which might be due to the interaction between the two semiconductors. With the further increase of the MoO<sub>3</sub> concentration, the BET value decreased from 14.7 m<sup>2</sup> g<sup>-1</sup> to 6.9 m<sup>2</sup> g<sup>-1</sup>. 15 wt% MoO<sub>3</sub>-g-C<sub>3</sub>N<sub>4</sub> sample presents the lowest specific surface area.

Fig. 2 shows the TEM pictures of g-C<sub>3</sub>N<sub>4</sub>, MoO<sub>3</sub>, and 1.5 wt% MoO<sub>3</sub>-g-C<sub>3</sub>N<sub>4</sub> composite. As shown in Fig. 2a, the morphology

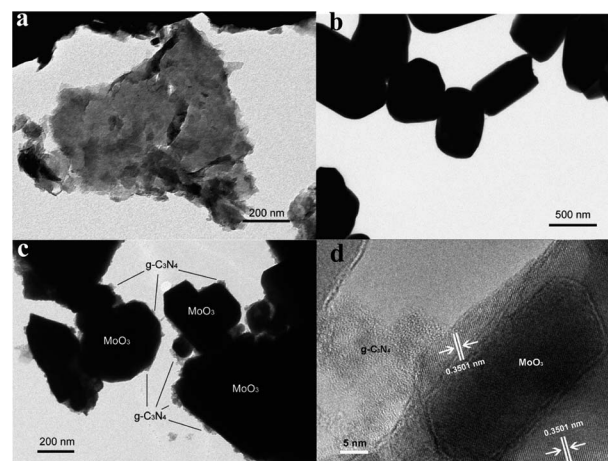


Fig. 2 TEM images of g-C<sub>3</sub>N<sub>4</sub> (a), MoO<sub>3</sub> (b), and 1.5 wt% MoO<sub>3</sub>-g-C<sub>3</sub>N<sub>4</sub> (c and d) photocatalysts.



of pure  $g\text{-C}_3\text{N}_4$  seems to be smooth, which is also confirmed by SEM observation (Fig. S2a†). The layer structure might be the origin of the special morphology of  $g\text{-C}_3\text{N}_4$ . Different from  $g\text{-C}_3\text{N}_4$ ,  $\text{MoO}_3$  sample had a particle size of 200–600 nm, and a grain-like morphology with polygonal grain shapes (Fig. 2b and S2b†). For the  $\text{MoO}_3\text{-}g\text{-C}_3\text{N}_4$  composite, several  $\text{MoO}_3$  particles were sparsely observed on the  $g\text{-C}_3\text{N}_4$  surface (Fig. S2c†), and almost all particles were in direct contact with the  $g\text{-C}_3\text{N}_4$ . The TEM image of  $\text{MoO}_3\text{-}g\text{-C}_3\text{N}_4$  gives detailed information on the contact of the two semiconductors. As can be seen in Fig. 2c, the big black particles could be assigned to  $\text{MoO}_3$  grain, while  $g\text{-C}_3\text{N}_4$  closely adhered to the surface of  $\text{MoO}_3$ . The close contact can be observed more clearly in the high-resolution TEM image. As shown in Fig. 2d, two different phases were observed. The dark and big phase which exhibits fringes with an interplanar spacing of about 0.3501 nm can be indexed into the (040) plane of  $\text{MoO}_3$ , whereas another phase without fringes can be assigned to  $g\text{-C}_3\text{N}_4$ . Additionally, because the  $\text{MoO}_3\text{-}g\text{-C}_3\text{N}_4$  hybrids were ultrasonicated for 20 min before TEM analysis, the result in Fig. 2c and d indicates that the interaction between the  $\text{MoO}_3$  particles and  $g\text{-C}_3\text{N}_4$  is very strong, which is beneficial to the formation of hetero-junction of  $\text{MoO}_3$  and  $g\text{-C}_3\text{N}_4$ .

The structure of  $\text{MoO}_3\text{-}g\text{-C}_3\text{N}_4$  composites was characterized by XRD and FT-IR. Fig. 3 shows the XRD patterns of  $\text{MoO}_3$ ,  $g\text{-C}_3\text{N}_4$ , and  $\text{MoO}_3\text{-}g\text{-C}_3\text{N}_4$  composites with different  $\text{MoO}_3$  concentration. Pure  $g\text{-C}_3\text{N}_4$  shows two broad peaks at  $2\theta = 13.0^\circ$  and  $27.4^\circ$ , which are the (001) and (002) diffraction planes of the graphite-like carbon nitride, respectively.<sup>13</sup> Pure  $\text{MoO}_3$  is in its orthorhombic phase (JCPDF 35-0609) and exhibits several strong diffraction peaks at  $2\theta = 12.8^\circ, 23.4^\circ, 25.7^\circ, 27.3^\circ, 33.8^\circ, 39.0^\circ$ .<sup>40</sup> In the  $\text{MoO}_3\text{-}g\text{-C}_3\text{N}_4$  composite, although the content of  $\text{MoO}_3$  is very low,  $\text{MoO}_3$  phase could still be observed due to its strong XRD signal. As  $\text{MoO}_3$  concentration increases from 1.0 wt% to 15 wt%, the diffraction peaks of  $\text{MoO}_3$  are gradually intensified, whereas the peaks of  $g\text{-C}_3\text{N}_4$  are weakened. This result accords well with that of TG experiment. With the exception of  $\text{MoO}_3$  and  $g\text{-C}_3\text{N}_4$ , no other phase was observed. The same result was also obtained in the FT-IR experiment. As shown in Fig. 4, pure  $g\text{-C}_3\text{N}_4$  shows strong IR signal in the range

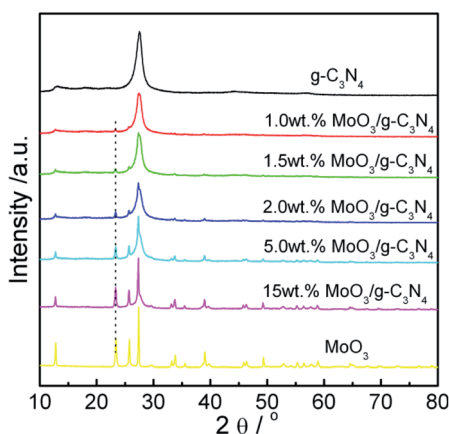


Fig. 3 XRD patterns of  $\text{MoO}_3\text{-}g\text{-C}_3\text{N}_4$  composites with different  $\text{MoO}_3$  concentration.

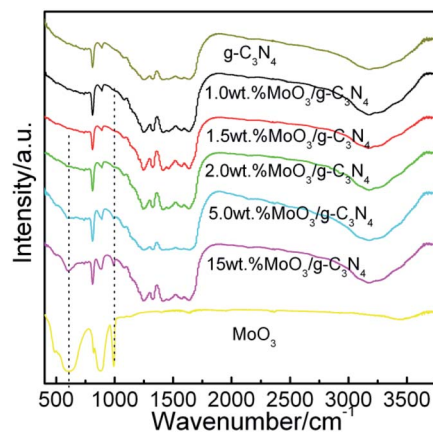


Fig. 4 FT-IR spectra of  $\text{MoO}_3\text{-}g\text{-C}_3\text{N}_4$  composites with different  $\text{MoO}_3$  concentration.

of  $1200\text{--}1600\text{ cm}^{-1}$ , which could be assigned to the  $\text{C}=\text{N}$  and aromatic  $\text{C}-\text{N}$  stretching vibration modes.<sup>41</sup> In addition, the signal of out-of plane bending modes of  $\text{C}-\text{N}$  heterocycle was also observed at  $808\text{ cm}^{-1}$ .<sup>41</sup> For  $\text{MoO}_3$ , only three strong IR peaks were observed. The peak at  $996\text{ cm}^{-1}$  could be assigned to the  $\text{Mo}=\text{O}$  stretching mode, while the peaks at  $562\text{ cm}^{-1}$  and  $859\text{ cm}^{-1}$  originate from the stretching mode of oxygen linked with three metal atoms and in the  $\text{Mo}-\text{O}-\text{Mo}$  units, respectively.<sup>42</sup> In the case of  $\text{MoO}_3\text{-}g\text{-C}_3\text{N}_4$  composite, the position of these characteristic peaks is as same as that of pure phase. The peak intensity of  $\text{MoO}_3$  increases with the  $\text{MoO}_3$  content, which is consistent with the results obtained with XRD.

XPS measurements were performed to explicate the valence states of various species. Fig. 5 shows the C1s high resolution XPS spectra of  $\text{MoO}_3$ ,  $g\text{-C}_3\text{N}_4$  and several  $\text{MoO}_3\text{-}g\text{-C}_3\text{N}_4$  composites. Pure  $g\text{-C}_3\text{N}_4$  has two C1s peak located at  $284.6\text{ eV}$

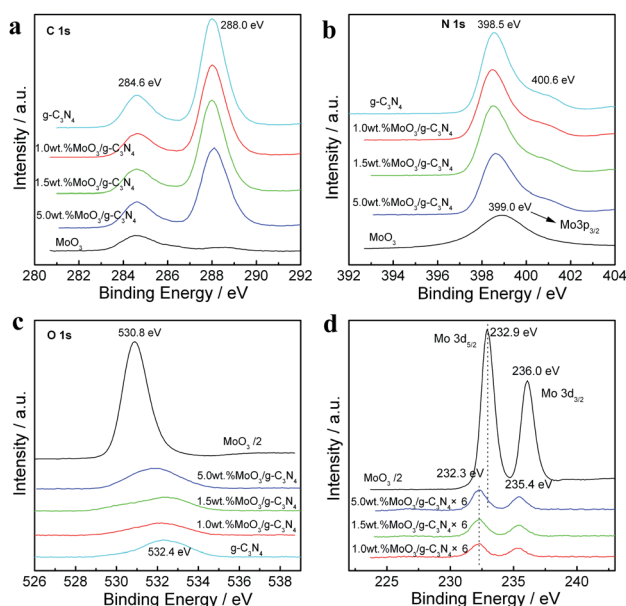


Fig. 5 XPS spectra of  $\text{MoO}_3$ ,  $g\text{-C}_3\text{N}_4$  and  $\text{MoO}_3\text{-}g\text{-C}_3\text{N}_4$  composites, (a) C1s; (b) N1s; (c) O1s and (d) Mo3d.

and 288.0 eV, which could be attributed to C–C coordination of carbon-containing contaminations and N–C–N coordination in graphitic carbon nitride, respectively.<sup>41</sup> For MoO<sub>3</sub>, only the contaminated carbon was observed. Hence, the C1s peak at 288.0 eV could be used to verify the existence of g-C<sub>3</sub>N<sub>4</sub> in the MoO<sub>3</sub>-g-C<sub>3</sub>N<sub>4</sub> photocatalyst. Generally, the N1s peak can also be the standard. The peak at 398.5 eV and 400.6 eV could be separately assigned to the nitrogen atoms in C–N–C and –NH<sub>x</sub> groups.<sup>41</sup> No shift was observed in the C1s or N1s peak after the addition of MoO<sub>3</sub> except a slight red shift of N1s in 15 wt% MoO<sub>3</sub>-g-C<sub>3</sub>N<sub>4</sub> sample. Li *et al.* observed the shift of N1s peak in 7 wt% g-C<sub>3</sub>N<sub>4</sub>-MoO<sub>3</sub> composite and attributed it to the interaction between Mo and N atoms.<sup>33</sup> However, it should be noted that the binding energy (BE) of Mo 3p<sub>3/2</sub> is very close to that of N1s. We think the contribution of Mo 3p<sub>3/2</sub> might be the reason of the N1s peak shift. Fig. 5c shows the high resolution XPS peak of O1s. MoO<sub>3</sub> has a strong O1s peak at 530.8 eV which could be attributed to the O<sup>2-</sup> in molybdenum oxide,<sup>43</sup> while g-C<sub>3</sub>N<sub>4</sub> has a small O1s peak originated from adsorbed H<sub>2</sub>O.<sup>41</sup> The O1s peak of MoO<sub>3</sub>-g-C<sub>3</sub>N<sub>4</sub> could be seen as the overlap of the two oxygen species. With the increase of the MoO<sub>3</sub> content, the position of O1s shifts to low binding energy end. The high-resolution XPS spectrum of Mo 3d exhibits the Mo (3d<sub>5/2</sub>, 3d<sub>3/2</sub>) doublet at 232.9 eV and 236.0 eV (Fig. 5d), the typical binding energies of Mo<sup>6+</sup>.<sup>44,45</sup> In the case of MoO<sub>3</sub>-g-C<sub>3</sub>N<sub>4</sub>, the BEs of Mo 3d<sub>5/2</sub> and Mo3d<sub>3/2</sub> are 232.3 and 235.4 eV, respectively. Earlier studies show that the Mo 3d<sub>5/2</sub> BE of MoO<sub>2</sub> is 229.6 eV, and the BE of Mo<sup>5+</sup> 3d<sub>5/2</sub> is 232.0 eV.<sup>44,45</sup> So, both Mo<sup>5+</sup> and Mo<sup>6+</sup> exist in the surface of MoO<sub>3</sub>-g-C<sub>3</sub>N<sub>4</sub> samples, although the XRD experiment indicates that molybdenum exists in the forms of crystalline MoO<sub>3</sub>. The Mo<sup>5+</sup> might originate from the catalytic oxidation of g-C<sub>3</sub>N<sub>4</sub> by MoO<sub>3</sub> during the preparation of MoO<sub>3</sub>-g-C<sub>3</sub>N<sub>4</sub>, which has been proven by the TG-DTA experiment (see Fig. S1†). Some Mo<sup>6+</sup> ions were reduced to Mo<sup>5+</sup> during the heating process. The reaction between g-C<sub>3</sub>N<sub>4</sub> and MoO<sub>3</sub> consumed some g-C<sub>3</sub>N<sub>4</sub>. Meanwhile, it promotes the interaction between the two semiconductors, which benefits the decrease in interface energy and the charge transfer between them. In addition, it could be observed that the change in MoO<sub>3</sub> concentration did not affect the BE of Mo3d<sub>5/2</sub>, which suggests that the surface Mo<sup>5+</sup> concentration is stable in the MoO<sub>3</sub>-g-C<sub>3</sub>N<sub>4</sub> composites. The surface phase composition of the 1.5 wt% MoO<sub>3</sub>-g-C<sub>3</sub>N<sub>4</sub> sample was obtained based on the XPS spectra. The MoO<sub>3</sub> concentration of the sample (Table S1†) is 1.0 mol%, which is close to 1.2 mol% (obtained with TG). This result indicates well dispersion of MoO<sub>3</sub> in composite, benefiting the formation of heterojunction structure between MoO<sub>3</sub> and g-C<sub>3</sub>N<sub>4</sub>. The valence band (VB) XPS spectra of g-C<sub>3</sub>N<sub>4</sub> and MoO<sub>3</sub> are shown in Fig. 6. The position of the valence band edges of g-C<sub>3</sub>N<sub>4</sub> and MoO<sub>3</sub> are 1.53 eV and 3.20 eV, respectively.

Fig. 7 shows the UV-vis DRS spectra of MoO<sub>3</sub>-g-C<sub>3</sub>N<sub>4</sub> composites. Only the spectra of 1.5 wt% MoO<sub>3</sub>-g-C<sub>3</sub>N<sub>4</sub> and 15 wt% MoO<sub>3</sub>-g-C<sub>3</sub>N<sub>4</sub> photocatalysts are presented. For all samples, the optical absorption edge was estimated to be at around 470 nm. This is consistent with their pale yellow color. Pure g-C<sub>3</sub>N<sub>4</sub> has the best photoabsorption performance. The band gap was estimated to be 2.70 eV based on the K–M equation.<sup>46</sup> The band

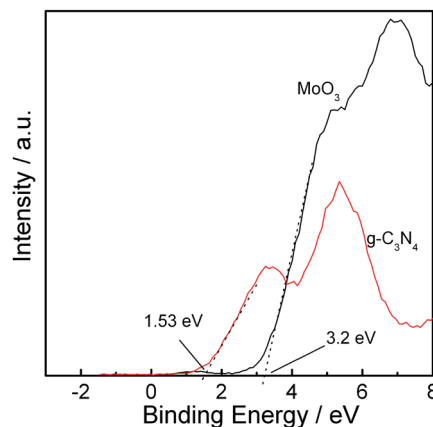


Fig. 6 Valence band XPS of MoO<sub>3</sub> and g-C<sub>3</sub>N<sub>4</sub>.

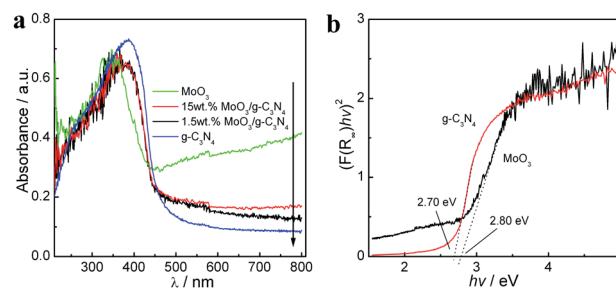


Fig. 7 UV-vis spectra of MoO<sub>3</sub>-g-C<sub>3</sub>N<sub>4</sub> (a) composites and the estimated band gaps of g-C<sub>3</sub>N<sub>4</sub> and MoO<sub>3</sub> (b).

gap of MoO<sub>3</sub> is 2.80 eV. Both accord well with the reported values.<sup>13,45</sup> The optical properties of MoO<sub>3</sub>-g-C<sub>3</sub>N<sub>4</sub> fall in between those of MoO<sub>3</sub> and g-C<sub>3</sub>N<sub>4</sub>. However, due to the low concentration of MoO<sub>3</sub> and the similar band gap of the two semiconductors, the composites with different MoO<sub>3</sub> contents exhibit nearly same photoabsorption performance.

### 3.2 Photocatalytic activities of g-C<sub>3</sub>N<sub>4</sub>, MoO<sub>3</sub>, and MoO<sub>3</sub>-g-C<sub>3</sub>N<sub>4</sub>

To evaluate the photocatalytic activity of as-prepared MoO<sub>3</sub>-g-C<sub>3</sub>N<sub>4</sub> composites, the degradation of MO was carried out. Fig. 8a

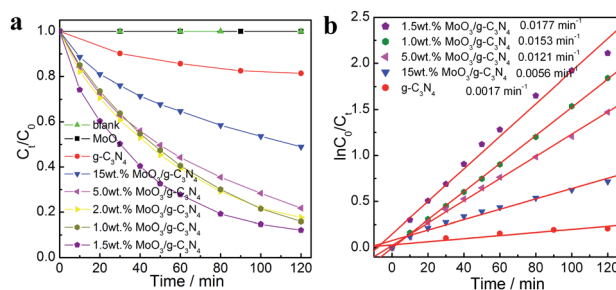


Fig. 8 Photocatalytic activities of MoO<sub>3</sub>-g-C<sub>3</sub>N<sub>4</sub> composites on photodegradation of MO under visible-light irradiation (a) and the corresponding kinetic studies (b). (Catalyst's content: 1.0g L<sup>-1</sup>; MO content: 20 ppm).

displays the changes of the MO concentration *versus* the reaction time over MoO<sub>3</sub>-g-C<sub>3</sub>N<sub>4</sub> photocatalysts prepared with different MoO<sub>3</sub> concentrations. The blank test shows that MO is stable under visible light irradiation, indicating that the photolysis of MO is negligible. MoO<sub>3</sub> barely shows activity for MO photodegradation, while g-C<sub>3</sub>N<sub>4</sub> demonstrates good photocatalytic activity with a degradation rate of 0.0017 min<sup>-1</sup> (Fig. 8b). The rate was estimated based on

$$\ln(C_0/C_t) = kt \quad (1)$$

where  $C_0$  is the equilibrium concentration of MO after 60 min dark adsorption,  $C_t$  is the MO concentration remaining in the solution at irradiation time  $t$  (min), and  $k$  is the observed rate constant.<sup>28,29</sup> The addition of MoO<sub>3</sub> to g-C<sub>3</sub>N<sub>4</sub> promotes the degradation of MO effectively. With the increase in MoO<sub>3</sub> concentration, the photocatalytic activity of MoO<sub>3</sub>-g-C<sub>3</sub>N<sub>4</sub> increases and then decreases. 1.5 wt% MoO<sub>3</sub>-g-C<sub>3</sub>N<sub>4</sub> exhibits the highest photocatalytic efficiency. The  $k$  value is 0.0177 min<sup>-1</sup> which is 10.4 times higher than that of pure g-C<sub>3</sub>N<sub>4</sub>. Obviously, the coupling of MoO<sub>3</sub> and g-C<sub>3</sub>N<sub>4</sub> creates an excellent composite photocatalyst. Considering that the MoO<sub>3</sub>-g-C<sub>3</sub>N<sub>4</sub> composites have similar specific surface area with g-C<sub>3</sub>N<sub>4</sub>, the enhanced photoactivity may be ascribed to the improvement in charge transmission between the semiconductors g-C<sub>3</sub>N<sub>4</sub> and MoO<sub>3</sub> prolonged the lifetime of charge carriers. Moreover, the photoactivity of the coupled semiconductors was also affected by the surface contact between particles. 1.5 wt% MoO<sub>3</sub>-g-C<sub>3</sub>N<sub>4</sub> might have the highest contact interfaces between MoO<sub>3</sub> and g-C<sub>3</sub>N<sub>4</sub>, and thus the highest photocatalytic efficiency.

Reaction conditions also have great effects on the photocatalytic reaction. The optimal reaction condition could accelerate the photocatalytic oxidation of dye. Therefore, in order to degrade MO more efficiently, the 1.5 wt% MoO<sub>3</sub>-g-C<sub>3</sub>N<sub>4</sub> sample was employed for the following investigations. It can be seen from Fig. 9a that the degradation rate of MO increased from 0.0145 min<sup>-1</sup> to 0.0210 min<sup>-1</sup> with catalyst amount, and then decreased slightly. Higher catalyst amount means higher availability of total surface area and active sites of the catalyst, and thus better adsorption of MO and degradation rate. However, when the catalyst is overdosed, the reductions in light penetration and light scattering would result in a reduction of degradation rate. An optimal amount (2.0 g L<sup>-1</sup>) was chosen for the further study. Fig. 9b shows the effect of the initial

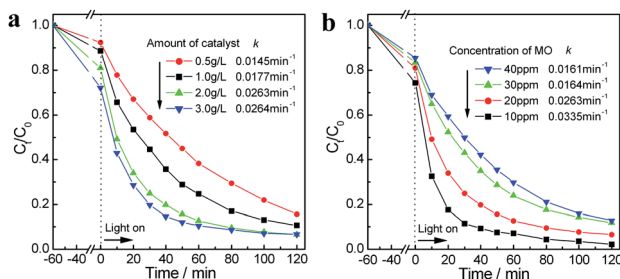


Fig. 9 Effect of catalyst content (a) and initial dye concentration (b) on the degradation of MO.

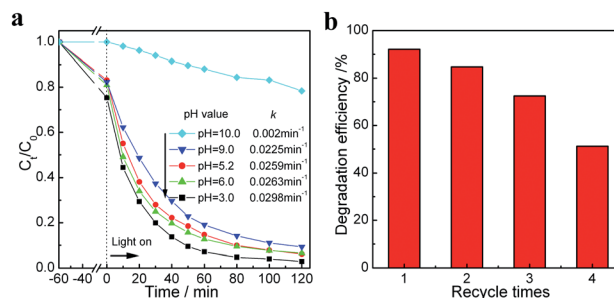


Fig. 10 Effect of the pH value of MO solution on the degradation of MO (a) and the cycling run of 1.5 wt% MoO<sub>3</sub>-g-C<sub>3</sub>N<sub>4</sub> (b). (Content of catalyst: 2.0 g L<sup>-1</sup>; content of MO: 20 ppm).

concentration of MO on the photocatalytic degradation of MO over 1.5 wt% MoO<sub>3</sub>-g-C<sub>3</sub>N<sub>4</sub> composite. The increase in MO concentration reduces the degradation efficiency, which might be due to the light attenuation in MO solution or the visible light screening effect of the dye. The higher the MO concentration is, the fewer the light could pass through the MO solution and reach the photocatalyst, and lead to lower photoactivity.

The influence of the pH on the photocatalytic degradation of MO was also investigated and the results are shown in Fig. 10a. When the pH value was lower than 9, pH had little effect on the photocatalytic oxidation of MO. The 1.5 wt% MoO<sub>3</sub>-g-C<sub>3</sub>N<sub>4</sub> photocatalyst exhibited good photoactivity in both neutral and acid solution. However, when pH was higher than 9, the photocatalytic activity decreased considerably. The loss of MoO<sub>3</sub> might result in the decrease in photoactivity, which was also observed in cyclic experiments. As shown in Fig. 10b, the degradation efficiency of 1.5 wt% MoO<sub>3</sub>-g-C<sub>3</sub>N<sub>4</sub> composite decreased gradually with the increase in the number of cyclic test. In the fourth run, only 55% of the initial activity was obtained. According to the results of XRD experiments, the disappearance of MoO<sub>3</sub> phase might lead to the inactivation of the photocatalyst (Fig. S2†). Unlike WO<sub>3</sub>, MoO<sub>3</sub> has very low solubility in water (4.9 g L<sup>-1</sup>, 28 °C). Although the strong interaction between g-C<sub>3</sub>N<sub>4</sub> and MoO<sub>3</sub> might slow down the dissolution process, the inactivation of the MoO<sub>3</sub>-g-C<sub>3</sub>N<sub>4</sub> is observed. It should be noted that the inactivation of MoO<sub>3</sub>-containing photocatalyst has not been reported before. All researchers claimed that the synthesized MoO<sub>3</sub>-containing photocatalyst is stable and can be recycled with water purification.<sup>32,33,47,48</sup> The observation might result from the high concentration of MoO<sub>3</sub> in those photocatalysts. MoO<sub>3</sub> dissolution did not affect photocatalytic activity during the several cyclic tests. However, it is no doubt that the inactivation of MoO<sub>3</sub>-containing photocatalyst during water purification is unavoidable due to the solubility of MoO<sub>3</sub>. The MoO<sub>3</sub>-containing composites are more suitable for air purification such as the photodegradation of acetone with SO<sub>4</sub><sup>2-</sup>-MoO<sub>3</sub>-MgF<sub>2</sub> composite.<sup>41</sup>

Fig. 11a shows the photocatalytic activity of MO, MB, and RhB in the presence of 1.5 wt% MoO<sub>3</sub>-g-C<sub>3</sub>N<sub>4</sub> composite. It can be seen that the MB and RhB dyes can also be photodegraded



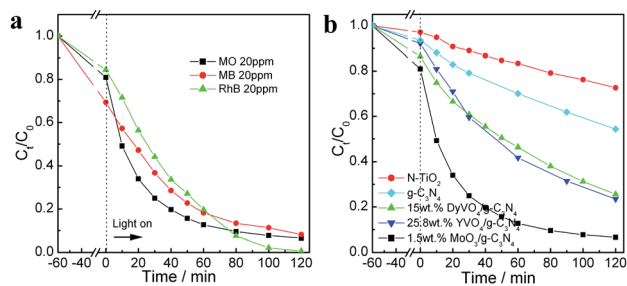


Fig. 11 The photodegradation of different organics over 1.5wt% MoO<sub>3</sub>-g-C<sub>3</sub>N<sub>4</sub> sample (a) and the photodegradation of MO over different photocatalysts (b). (Content of catalyst: 2.0g L<sup>-1</sup>; pH = 6.0).

efficiently over the MoO<sub>3</sub>-g-C<sub>3</sub>N<sub>4</sub> photocatalyst besides MO. Indeed, many photocatalysts could only degrade one type of dye. For example, it was reported that CaBi<sub>6</sub>O<sub>10</sub>/Bi<sub>2</sub>O<sub>3</sub> photocatalyst is only effective in RhB photodegradation.<sup>34</sup> Yan *et al.* found that pure g-C<sub>3</sub>N<sub>4</sub> exhibited much higher photocatalytic activity in RhB degradation than that in MO degradation.<sup>49</sup> The result in Fig. 11a indicates the general applicability of the synthesized MoO<sub>3</sub>-g-C<sub>3</sub>N<sub>4</sub> photocatalyst since RhB and MO are two different type of dyes. Fig. 11b displays the photocatalytic activities of different photocatalysts in photodegradation of MO. Actually, the g-C<sub>3</sub>N<sub>4</sub>-MoO<sub>3</sub> and WO<sub>3</sub>-g-C<sub>3</sub>N<sub>4</sub> composite photocatalysts were also prepared based on the reported literature.<sup>25,33</sup> However, the synthesized photocatalysts display different photocatalytic behavior from the literature, which might be due to the inconsistency in preparation techniques and experimental conditions. Hence, in order to eliminate their effects, only the N-TiO<sub>2</sub>,<sup>34</sup> DyVO<sub>4</sub>/g-C<sub>3</sub>N<sub>4</sub>,<sup>38</sup> and YVO<sub>4</sub>/g-C<sub>3</sub>N<sub>4</sub> (ref. 31) photocatalysts which we have previously reported were chosen as the reference photocatalysts. The result shown in Fig. 11b demonstrated the superiority of MoO<sub>3</sub>-g-C<sub>3</sub>N<sub>4</sub> composite. The MoO<sub>3</sub>-g-C<sub>3</sub>N<sub>4</sub> photocatalyst had better performance on photocatalytic oxidation of MO than the other g-C<sub>3</sub>N<sub>4</sub> based photocatalysts.

Therefore, the synthesized MoO<sub>3</sub>-g-C<sub>3</sub>N<sub>4</sub> composite is an excellent photocatalyst for the photodegradation of MO, RhB, and MB. The addition of a small amount of MoO<sub>3</sub> could greatly promote the photocatalytic activity of g-C<sub>3</sub>N<sub>4</sub>. The highest photocatalytic activity could be obtained by optimizing the influencing factors (MoO<sub>3</sub> concentration, catalyst amount, initial MO concentration, pH of MO solution). However, MoO<sub>3</sub>-g-C<sub>3</sub>N<sub>4</sub> composite is not stable in water. In order to make it applicable for water purification, the modification should be done, which includes coating the exposed MoO<sub>3</sub> surface with a nanocarbon layer to prevent the dissolution of MoO<sub>3</sub>.

### 3.3 Possible mechanism of enhanced photocatalytic activity of MoO<sub>3</sub>-g-C<sub>3</sub>N<sub>4</sub> composite

Although the surface area of a photocatalyst has been considered as an important factor in determining the photocatalytic activity, the separation efficiency of electron-hole pairs of the composite photocatalyst including MoO<sub>3</sub>-g-C<sub>3</sub>N<sub>4</sub> used in this research is always the key factor. The excellent photocatalytic activity is associated with the enhanced separation efficiency resulting from the addition of

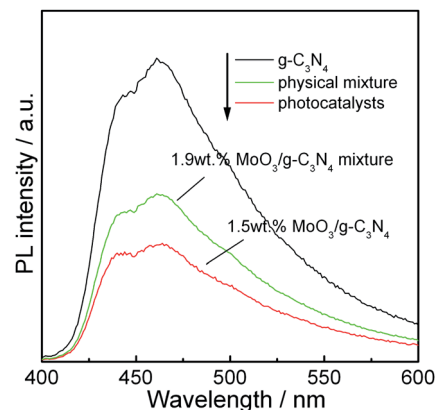


Fig. 12 Photoluminescence spectra of pure g-C<sub>3</sub>N<sub>4</sub>, 1.5 wt% MoO<sub>3</sub>-g-C<sub>3</sub>N<sub>4</sub> composite, and 1.9 wt% MoO<sub>3</sub>-g-C<sub>3</sub>N<sub>4</sub> physical mixture.

MoO<sub>3</sub>. XPS experiment shows that some Mo<sup>5+</sup> species formed on the surface of the composite might contribute to the separation of electron-hole pairs because Mo<sup>5+</sup> has been reported to be the low trap of hole.<sup>7,45</sup> However, due to the inconsistency of surface Mo<sup>5+</sup> content and photoactivity, the coupling effect between MoO<sub>3</sub> and g-C<sub>3</sub>N<sub>4</sub> should be the main reason, suppressing the recombination of electron-hole pairs, and subsequently improving the photocatalytic efficiency. The PL experiment was carried out to confirm the assumption. Fig. 12 shows the PL spectra of pure g-C<sub>3</sub>N<sub>4</sub>, 1.5 wt% MoO<sub>3</sub>-g-C<sub>3</sub>N<sub>4</sub> composite, and 1.9 wt% MoO<sub>3</sub>-g-C<sub>3</sub>N<sub>4</sub> mixture. The mixture containing the same amount of MoO<sub>3</sub> as the 1.5 wt% MoO<sub>3</sub>-g-C<sub>3</sub>N<sub>4</sub> sample was prepared as a reference catalyst. G-C<sub>3</sub>N<sub>4</sub> has a strong PL emission at about 460 nm, an indication of rapid recombination of electrons and holes.<sup>50</sup> The other two samples have a PL peak at the same position. The peak intensities of three materials are in the order of g-C<sub>3</sub>N<sub>4</sub> > 1.9 wt% MoO<sub>3</sub>-g-C<sub>3</sub>N<sub>4</sub> mixture > 1.5 wt% MoO<sub>3</sub>-g-C<sub>3</sub>N<sub>4</sub> composite. In general, the surface energies of MoO<sub>3</sub> and g-C<sub>3</sub>N<sub>4</sub> in the mixture should be high due to the lack of calcination, which retards the interparticle electron transfer. Hence, the weak PL intensity of 1.9 wt% MoO<sub>3</sub>-g-C<sub>3</sub>N<sub>4</sub> mixture could be mainly ascribed to the decrease in g-C<sub>3</sub>N<sub>4</sub> concentration. The fact that PL peak of the 1.5 wt% MoO<sub>3</sub>-g-C<sub>3</sub>N<sub>4</sub> composite is weaker than that of the physical mixture verifies the existence of the charge transfer between MoO<sub>3</sub> and g-C<sub>3</sub>N<sub>4</sub> particles.

The PT experiments were also carried out to reveal dynamics of the charge transfer between the interfacial surface of MoO<sub>3</sub> and g-C<sub>3</sub>N<sub>4</sub> semiconductors. As shown from Fig. 13, the photocurrent of 1.5 wt% MoO<sub>3</sub>-g-C<sub>3</sub>N<sub>4</sub> is much higher than that of g-C<sub>3</sub>N<sub>4</sub> or MoO<sub>3</sub>, thus holds stronger ability in generating and transferring the photoexcited charge carrier under visible light irradiation.<sup>51,52</sup> The results in Fig. 13 are well in agreement with those from the PL experiments.

Therefore, it is obvious that the efficient charge separation is the origin of the high photoactivity of MoO<sub>3</sub>-g-C<sub>3</sub>N<sub>4</sub>. However, the associated mechanism is unclear. Based on

$$E_{cb} = E_g - E_{vb} \quad (2)$$

and the results of VB XPS and DRS, the band edge potentials of MoO<sub>3</sub> and g-C<sub>3</sub>N<sub>4</sub> could be determined. The sensitization

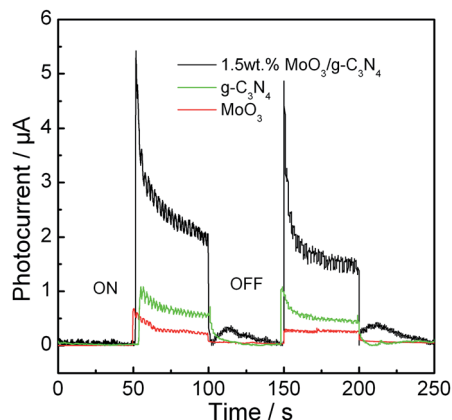


Fig. 13 Transient photocurrent responses for  $g\text{-C}_3\text{N}_4$  and 1.5 wt%  $\text{MoO}_3\text{-}g\text{-C}_3\text{N}_4$  photocatalysts.

mechanism should be excluded since both  $\text{MoO}_3$  and  $g\text{-C}_3\text{N}_4$  have visible light absorption ability. However, the final determination of the working mechanism of the  $\text{MoO}_3\text{-}g\text{-C}_3\text{N}_4$  photocatalyst is still difficult because the band potentials of  $\text{MoO}_3$  and  $g\text{-C}_3\text{N}_4$  meet the requirements of both mechanisms (Fig. 14). Li *et al.* reported that  $g\text{-C}_3\text{N}_4\text{-MoO}_3$  composite follows the double charge transfer mechanism (Fig. 14a).<sup>33</sup> This mechanism was also thought to work in another similar photocatalyst,  $\text{WO}_3/g\text{-C}_3\text{N}_4$  composite.<sup>25,53</sup> But these authors did not consider the possibility of Z-scheme type mechanism. Meanwhile, some studies showed that the photogenerated electrons migrate by the Z-scheme route in the  $\text{MoO}_3$ -containing composite photocatalysts ( $\text{MoO}_3/\text{TiO}_2\text{-}x\text{S}_x$ ,<sup>32</sup>  $\text{Pt/MoO}_3/\text{TiO}_2$ ,<sup>54</sup>  $\text{MoO}_3\text{-TiO}_2$  (ref. 55)). The theory is based on the assumption that the photocatalytic efficiency of the Z-scheme photocatalysis system is limited by the semiconductor with a wider band gap.<sup>56</sup> However, due to the similarity band gaps of  $\text{MoO}_3$  and  $g\text{-C}_3\text{N}_4$ , a new method is needed to determine the function mechanism of  $\text{MoO}_3\text{-}g\text{-C}_3\text{N}_4$ .

The activity of a photocatalyst originates from the redox ability of electrons and holes.<sup>1,2</sup> The band potentials of a semiconductor greatly affect the photocatalytic reaction. Actually, band potential difference was considered as an important reason of the higher photoactivities of  $\text{BiOCl}$  and  $\text{Zn}_2\text{GeO}_4$  than that of  $\text{P25}$ .<sup>57,58</sup> However, for composite photocatalysts, the

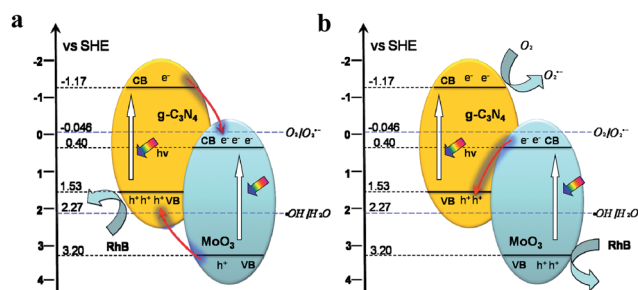


Fig. 14 Possible schemes for electron-hole separation and transport at the visible-light-driven  $\text{MoO}_3\text{-}g\text{-C}_3\text{N}_4$  composite interface: (a) double charge transfer mechanism, (b) Z-Scheme mechanism.

positive effect of charge separation is great enough to control the photocatalytic reaction. The effect of the change in redox ability resulting from the charge migration is usually neglected. Migration does influence the process of the photocatalytic oxidation of organics. For example, although the photocatalytic activity of  $g\text{-C}_3\text{N}_4$  was greatly improved due to the addition of  $\text{GdVO}_4$ , the  $\cdot\text{OH}$  concentration in the presence of  $\text{GdVO}_4/g\text{-C}_3\text{N}_4$  composite is lower than that of pure  $g\text{-C}_3\text{N}_4$  and  $\text{GdVO}_4$ .<sup>59</sup> This change in the content of reactive species could be attributed to the decrease in redox potentials of electron and holes. Hence, in the case of  $\text{MoO}_3\text{-}g\text{-C}_3\text{N}_4$  composite, the change in redox ability can affect the reactive species. If the  $\text{MoO}_3\text{-}g\text{-C}_3\text{N}_4$  photocatalyst follows the same mechanism as  $\text{GdVO}_4/g\text{-C}_3\text{N}_4$  composite (double charge transfer mechanism, Fig. 14 a), the decrease in  $\cdot\text{OH}$  concentration would be observed over  $\text{MoO}_3\text{-}g\text{-C}_3\text{N}_4$  composite. In addition, due to the conduction band potential of  $\text{MoO}_3$  is lower than the standard reduction potential of  $\cdot\text{O}_2^-/\text{O}_2$ , the electron transfer from the CB of  $g\text{-C}_3\text{N}_4$  to that of  $\text{MoO}_3$  would lead to the significant decrease in  $\cdot\text{O}_2^-$  concentration. It would be impossible that the  $\text{MoO}_3\text{-}g\text{-C}_3\text{N}_4$  composite and pure  $g\text{-C}_3\text{N}_4$  have the same dominant reactive species  $\cdot\text{O}_2^-$ . On the contrary, if the  $\text{MoO}_3\text{-}g\text{-C}_3\text{N}_4$  follows the Z-scheme type mechanism, the opposite result would be obtained.

Fig. 15 shows the kinetic constants of  $g\text{-C}_3\text{N}_4$  and 1.5 wt%  $\text{MoO}_3\text{-}g\text{-C}_3\text{N}_4$  photocatalyst in the presence of different quenchers. The addition of benzoquinone (BQ,  $\cdot\text{O}_2^-$  scavenger) greatly decreased the photocatalytic activity of  $g\text{-C}_3\text{N}_4$ , indicating that  $\cdot\text{O}_2^-$  is the dominant active species,<sup>35,36</sup> which is consistent with the Ji's work.<sup>60</sup> A small decrease in  $k$  was also observed after the addition of KI (KI,  $\cdot\text{OH}$  and  $h^+$  scavenger),<sup>35,36</sup> whereas isopropanol (IPA, a quencher of  $\cdot\text{OH}$ ) has nearly no effect on the degradation of MO in the presence of  $g\text{-C}_3\text{N}_4$  catalyst.<sup>35,36</sup> For the  $\text{MoO}_3\text{-}g\text{-C}_3\text{N}_4$  composite, similar results were obtained. The active trapping experiments verified that  $\cdot\text{O}_2^-$  and  $h^+$  are the reactive species during the photocatalytic oxidation of MO. Thus,  $\text{MoO}_3\text{-}g\text{-C}_3\text{N}_4$  composite photocatalyst follows the direct Z-scheme type mechanism. Besides, it could be noted that the isopropanol scavenger displayed a stronger effect on the photoactivity of  $\text{MoO}_3\text{-}g\text{-C}_3\text{N}_4$  than that of  $g\text{-C}_3\text{N}_4$ . This phenomenon suggests the increase in  $\cdot\text{OH}$  concentration

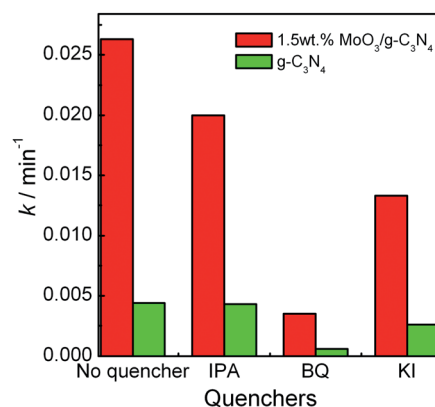


Fig. 15 Kinetic constants of  $g\text{-C}_3\text{N}_4$  and 1.5 wt%  $\text{MoO}_3\text{-}g\text{-C}_3\text{N}_4$  photocatalyst with different quenchers.



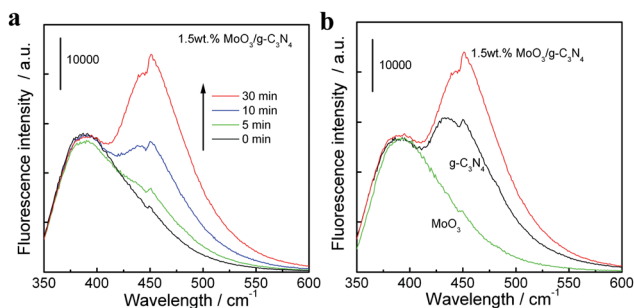


Fig. 16  $\cdot\text{OH}$ -trapping photoluminescence spectra of photocatalyst under visible-light irradiation in a solution of COU at room temperature (a) 1.5 wt%  $\text{MoO}_3\text{-g-C}_3\text{N}_4$ . (b)  $\text{MoO}_3$ ,  $\text{g-C}_3\text{N}_4$ , and 1.5 wt%  $\text{MoO}_3\text{-g-C}_3\text{N}_4$  samples under light irradiation for 30 min.

in the  $\text{MoO}_3\text{-g-C}_3\text{N}_4$  composite, which is in a good agreement with the expectation of the Z-scheme mechanism.

The increased  $\cdot\text{OH}$  concentration was verified via the experiments with the trapping of hydroxyl radicals ( $\cdot\text{OH}$ ) by COU. Fig. 16a displays the  $\cdot\text{OH}$ -trapping photoluminescence spectra of 1.5 wt%  $\text{MoO}_3\text{-g-C}_3\text{N}_4$  composite under visible-light irradiation. PL emission peak at approximately 456 nm was observed and gradually increased with prolonged irradiation time, which indicates that the  $\cdot\text{OH}$  was photogenerated.<sup>37</sup> The PL spectra of  $\text{MoO}_3$ ,  $\text{g-C}_3\text{N}_4$  and 1.5 wt%  $\text{MoO}_3\text{-g-C}_3\text{N}_4$  samples under visible light irradiation for 30 min are shown in Fig. 16b. The 1.5 wt%  $\text{MoO}_3\text{-g-C}_3\text{N}_4$  sample has the strongest PL peak, indicating that  $\cdot\text{OH}$  concentration was higher than that of pure  $\text{g-C}_3\text{N}_4$ . Obviously, due to the high concentrations of the electron on the CB of  $\text{g-C}_3\text{N}_4$  and holes on the VB of  $\text{MoO}_3$ , and thus ease in the generation of  $\cdot\text{OH}$  species. The data in Fig. 15 and 16 clearly verifies that Z-scheme type mechanism is applicable to the  $\text{MoO}_3\text{-g-C}_3\text{N}_4$  composite photocatalyst.

## 4. Conclusion

The prepared  $\text{MoO}_3\text{-g-C}_3\text{N}_4$  powders exhibited excellent performance in the degradation of MO, RhB and MB, and displayed much higher photocatalytic activity than single  $\text{g-C}_3\text{N}_4$  or  $\text{MoO}_3$  under visible-light irradiation ( $>420$  nm). The synergic effect of  $\text{g-C}_3\text{N}_4$  and  $\text{MoO}_3$  was considered as the origin of the high activity of  $\text{MoO}_3\text{-g-C}_3\text{N}_4$  composite. However, due to the very low solubility of  $\text{MoO}_3$ , the deactivation of the photocatalyst in water is unavoidable. The photocatalyst containing  $\text{MoO}_3$  might be more suitable for the air purification. In addition, the reactive species trapping experiment and the coumarin photoluminescence probing technique were used for verification of the Z-scheme mechanism of  $\text{MoO}_3\text{-g-C}_3\text{N}_4$  composite. The method employed in this research could help researchers study the photocatalytic mechanism of new composite photocatalyst.

## Acknowledgements

We acknowledge Dr Xiaodong Yi in Xiamen University for his help in XPS analysis. This work was financially supported by the

National Natural Science Foundation of China (21003109, 51108424), the Opening-foundation of State Key Laboratory Physical Chemistry and Solid Surfaces, Xiamen University, China (201311), and the School of Energy Resources at University of Wyoming.

## Notes and references

- 1 S. Malato, J. Blanco, A. Vidal and C. Richter, *Appl. Catal., B*, 2002, **37**, 1–15.
- 2 A. Fujishima, T. N. Rao and D. A. Tryk, *J. Photochem. Photobiol., C*, 2000, **1**, 1–21.
- 3 S. Kwon, M. Fan, A. T. Cooper and H. Yang, *Crit. Rev. Environ. Sci. Technol.*, 2008, **38**, 197–226.
- 4 J. Qu and M. Fan, *Crit. Rev. Environ. Sci. Technol.*, 2010, **40**, 519–560.
- 5 H. Hu, Q. Yang, X. Lu, W. Wang, S. Wang and M. Fan, *Crit. Rev. Environ. Sci. Technol.*, 2010, **40**, 452–518.
- 6 T. Li, Y. Chen, P. Wan, M. Fan and X. Yang, *J. Am. Chem. Soc.*, 2009, **132**, 2500–2501.
- 7 W. Choi, A. Termin and M. R. Hoffmann, *J. Phys. Chem.*, 1994, **98**, 13669–13679.
- 8 J. Zhang, C. X. Pan, P. F. Fang, J. H. Wei and R. Xiong, *ACS Appl. Mater. Interfaces*, 2010, **2**, 1173–1176.
- 9 R. Ashi, T. Morikawa, T. Ohwaki, K. Aoki and Y. Taga, *Science*, 2001, **293**, 269–271.
- 10 G. H. Qin, Z. Sun, Q. P. Wu, L. Lin, M. Liang and S. Xue, *J. Hazard. Mater.*, 2011, **192**, 599–604.
- 11 J. B. Mu, B. Chen, M. Y. Zhang, Z. C. Guo, P. Zhang, Z. Y. Zhang, Y. Y. Sun, C. L. Shao and Y. C. Liu, *ACS Appl. Mater. Interfaces*, 2012, **4**, 424–430.
- 12 A. K. P. Mann, E. M. P. Steinmiller and S. E. Skrabalak, *Dalton Trans.*, 2012, **41**, 7939–7945.
- 13 X. C. Wang, K. Maeda, A. Thomas, K. Takanebe, G. Xin, J. M. Carlsson, K. Domen and M. Antonietti, *Nat. Mater.*, 2009, **8**, 76–80.
- 14 Y. P. Bi, S. X. Ouyang, N. Umezawa, J. Y. Cao and J. H. Ye, *J. Am. Chem. Soc.*, 2011, **133**, 6490–6492.
- 15 P. Wang, B. B. Huang, X. Y. Zhang, X. Y. Qin, H. Jin, Y. Dai, Z. Y. Wang, J. Y. Wei, J. Zhan, S. Y. Wang, J. P. Wang and M. H. Whangbo, *Chem.-Eur. J.*, 2009, **15**, 1821–1824.
- 16 S. C. Yan, Z. S. Li and Z. G. Zou, *Langmuir*, 2009, **25**, 10397–10401.
- 17 G. Q. Li, N. Yang, W. L. Wang and W. F. Zhang, *J. Phys. Chem. C*, 2009, **113**, 14829–14833.
- 18 Y. J. Cui, J. H. Huang, X. Z. Fu and X. C. Wang, *Catal. Sci. Technol.*, 2012, **2**, 1396–1402.
- 19 S. C. Lee, H. O. Lintang and L. Yuliati, *Chem. – Asian J.*, 2012, **7**, 2139–2144.
- 20 G. Liu, P. Niu, C. H. Sun, S. C. Smith, Z. G. Chen, G. Q. Lu and H. M. Cheng, *J. Am. Chem. Soc.*, 2010, **132**, 11642–11648.
- 21 X. C. Wang, X. F. Chen, A. Thomas, X. Z. Fu and M. Antonietti, *Adv. Mater.*, 2009, **21**, 1609–1612.
- 22 S. C. Yan, S. B. Lv, Z. S. Li and Z. G. Zou, *Dalton Trans.*, 2010, **39**, 1488–1491.
- 23 Y. J. Wang, Z. X. Wang, S. Muhammad and J. He, *CrystEngComm*, 2012, **4**, 5065–5070.

- 24 J. H. Yang, H. J. Yan, X. L. Wang, F. Y. Wen, Z. J. Wang, D. Y. Fan, J. Y. Shi and C. Li, *J. Catal.*, 2012, **290**, 151–157.
- 25 L. Y. Huang, H. Xu, Y. P. Li, H. M. Li, X. N. Cheng, J. X. Xia, Y. G. Xu and G. B. Cai, *Dalton Trans.*, 2013, **42**, 8606–8616.
- 26 J. X. Sun, Y. P. Yuan, L. G. Qiu, X. Jiang, A. J. Xie, Y. H. Shen and J. F. Zhu, *Dalton Trans.*, 2012, **41**, 6756–6763.
- 27 T. T. Li, L. H. Zhao, Y. M. He, J. Cai, M. F. Luo and J. J. Lin, *Appl. Catal., B*, 2013, **129**, 255–263.
- 28 L. Ge, C. C. Han and J. Liu, *Appl. Catal., B*, 2011, **108**, 100–107.
- 29 H. Xu, J. Yan, Y. G. Xu, Y. H. Song, H. M. Li, J. X. Xia, C. J. Huang and H. L. Wan, *Appl. Catal., B*, 2013, **129**, 182–193.
- 30 H. J. Yan and H. X. Yang, *J. Alloys Compd.*, 2011, **509**, L26–L29.
- 31 J. Cai, Y. M. He, X. X. Wang, L. H. Zhang, L. Z. Dong, H. J. Lin, L. H. Zhao, X. D. Yi, W. Z. Weng and H. L. Wan, *RSC Adv.*, 2013, **3**, 20862–20868.
- 32 K. Kondo, N. Murakami, C. Ye, T. Tsubota and T. Ohno, *Appl. Catal., B*, 2013, **142–143**, 362–367.
- 33 L. Y. Huang, H. Xu, R. X. Zhang, X. N. Cheng, J. X. Xia, Y. G. Xu and H. M. Li, *Appl. Surf. Sci.*, 2013, **283**, 25–32.
- 34 Y. J. Wang, Y. M. He, T. T. Li, J. Cai, M. F. Luo and L. H. Zhao, *Chem. Eng. J.*, 2012, **189–190**, 473–481.
- 35 G. T. Li, K. H. Wong, X. W. Zhang, C. Hu, J. C. Yu, R. C. Y. Chan and P. K. Wong, *Chemosphere*, 2009, **76**, 1185–1191.
- 36 J. Cao, B. Y. Xu, B. D. Luo, H. L. Lin and S. F. Chen, *Appl. Surf. Sci.*, 2011, **257**, 7083–7089.
- 37 Q. J. Xiang, J. G. Yu and P. K. Wong, *J. Colloid Interface Sci.*, 2011, **357**, 163–167.
- 38 Y. M. He, J. Cai, T. T. Li, Y. Wu, Y. M. Yi, L. H. Zhao and M. F. Luo, *Ind. Eng. Chem. Res.*, 2012, **51**, 14729–14737.
- 39 Y. M. He, J. Cai, T. T. Li, Y. Wu, H. J. Lin, L. H. Zhao and M. F. Luo, *Chem. Eng. J.*, 2013, **215–216**, 721–730.
- 40 T. H. Chiang and H. C. Yeh, *Materials*, 2013, **6**, 4609–4625.
- 41 H. J. Yan, Y. Chen and S. M. Xu, *Int. J. Hydrogen Energy*, 2012, **37**, 125–133.
- 42 F. Prinetto, G. Cerrato, G. Ghiotti, A. Chiorino, M. C. Campa, D. Gazzoli and V. Indovina, *J. Phys. Chem.*, 1995, **99**, 5556–5567.
- 43 B. M. Reddy, B. Chowdhury, E. P. Reddy and A. Fernández, *Appl. Catal., A*, 2001, **213**, 279–288.
- 44 K. Asakura, K. Nakatani, T. Kubota and Y. Iwasawa, *J. Catal.*, 2000, **194**, 309–317.
- 45 Y. M. He, L. H. Zhao, Y. J. Wang, T. T. Li, T. H. Wu, X. T. Wu and Y. Wu, *Ind. Eng. Chem. Res.*, 2011, **50**, 7109–7119.
- 46 H. J. Dong, G. Chen, J. X. Sun, C. M. Li, Y. G. Yu and D. H. Chen, *Appl. Catal., B*, 2013, **134–135**, 46–54.
- 47 S. M. Lam, J. C. Sin, A. Z. Abdullah and A. R. Mohamedt, *J. Mol. Catal. A: Chem.*, 2013, **370**, 123–131.
- 48 A. Chithambararaj, N. S. Sanjini, S. Velmathi and A. C. Bose, *Phys. Chem. Chem. Phys.*, 2013, **15**, 14761–14769.
- 49 S. C. Yan, Z. S. Li and Z. G. Zou, *Langmuir*, 2010, **26**, 3894–3901.
- 50 D. Z. Li, Z. X. Chen, Y. L. Chen, W. J. Li, H. J. Huang, Y. H. He and X. Z. Fu, *Environ. Sci. Technol.*, 2008, **42**, 2130–2135.
- 51 M. Kong, Y. Z. Li, X. Chen, T. T. Tian, P. F. Fang, F. Zheng and X. J. Zhao, *J. Am. Chem. Soc.*, 2011, **113**, 16414–16417.
- 52 Q. J. Xiang, J. G. Yu and M. Jaroniec, *J. Phys. Chem. C*, 2011, **115**, 7355–7363.
- 53 L. Y. Huang, H. Xu, Y. P. Li, H. M. Li, X. N. Cheng, J. X. Xia, Y. G. Xu and G. B. Cai, *Dalton Trans.*, 2013, **42**, 8606–8616.
- 54 B. J. Ma, J. S. Kim, C. H. Choi and S. I. Woo, *Int. J. Hydrogen Energy*, 2013, **38**, 3582–3587.
- 55 M. Navgire, A. Yelwande, D. Tayde, B. Arbad and M. Lande, *Chin. J. Catal.*, 2012, **33**, 261–266.
- 56 Y. Sasaki, H. Nemoto, K. Saito and A. Kudo, *J. Phys. Chem. C*, 2009, **113**, 17536–17542.
- 57 P. Ye, J. J. Xie, Y. M. He, L. Zhang, T. H. Wu and Y. Wu, *Mater. Lett.*, 2013, **108**, 168–171.
- 58 J. Liang, Y. Q. Cao, H. Lin, Z. Z. Zhang, C. C. Huang and X. X. Wang, *Inorg. Chem.*, 2013, **52**, 6916–6922.
- 59 Y. M. He, J. Cai, T. T. Li, Y. Wu, H. J. Lin, L. H. Zhao and M. F. Luo, *Chem. Eng. J.*, 2013, **215–216**, 721–730.
- 60 H. H. Ji, F. Chang, X. F. Hu, W. Qin and J. W. Shen, *Chem. Eng. J.*, 2013, **218**, 183–190.